

Dynamical He Flashes in Double White Dwarf Binaries

TIN LONG SUNNY WONG ¹ AND LARS BILDSTEN ^{1,2}

¹*Department of Physics, University of California, Santa Barbara, CA 93106, USA*

²*Kavli Institute for Theoretical Physics, University of California, Santa Barbara, CA 93106, USA*

ABSTRACT

The detonation of an overlying helium layer on a $0.8 - 1.1 M_{\odot}$ carbon-oxygen (CO) white dwarf (WD) can detonate the CO WD and create a thermonuclear supernova (SN). Many authors have recently shown that when the mass of the He layer is low ($\lesssim 0.03 M_{\odot}$), the ashes from its detonation minimally impact the spectra and light-curve from the CO detonation, allowing the explosion to appear remarkably similar to Type Ia SNe. These new insights motivate our investigation of dynamical He shell burning, and our search for a binary scenario that stably accumulates thermally unstable He shells in the $0.01 - 0.08 M_{\odot}$ range, thick enough to detonate, but also often thin enough for minimal impact on the observables. We first show that our improved non-adiabatic evolution of convective He shell burning in this shell mass range leads to conditions ripe for a He detonation. We also find that a stable mass-transfer scenario with a high entropy He WD donor of mass $0.15 - 0.25 M_{\odot}$ yields the He shell masses needed to achieve the double detonations. This scenario also predicts that the surviving He donor leaves with a space velocity consistent with the unusual runaway object, D6-2. We find that hot He WD donors originate in common envelope events when a $1.3 - 2.0 M_{\odot}$ star fills its Roche lobe at the base of the red giant branch at orbital periods of $1 - 10$ days with the CO WD.

1. INTRODUCTION

For decades astrophysicists have tried to answer the question – where do type Ia supernovae (SNe Ia) come from? The broadly accepted answer is that they come from the detonation of a carbon-oxygen white dwarf (CO WD) (Hoyle & Fowler 1960). However, it is unclear whether SNe Ia predominantly come from explosions occurring near the Chandrasekhar mass (M_{Ch}), or below.

One proposed sub- M_{Ch} explosion mechanism is the double detonation scenario, where the detonation of a He shell triggers the detonation of the underlying CO core (e.g., Livne 1990; Livne & Glasner 1991; Woosley & Weaver 1994; García-Senz et al. 1999; Fink et al. 2007, 2010; Kromer et al. 2010; Woosley & Kasen 2011; Sim et al. 2012; Pakmor et al. 2012; Moll & Woosley 2013; Shen & Bildsten 2014; Townsley et al. 2019; Polin et al. 2019; Gronow et al. 2020; Leung & Nomoto 2020; Boos et al. 2021; Gronow et al. 2021). A challenge to this scenario is that the burning products of the He shell detonation lead to disagreements in spectra and light

curve with observations of normal SNe Ia (e.g., Hoeflich & Khokhlov 1996; Nugent et al. 1997); the production of Ti, Cr and Fe group elements in the He detonation leads to line blanketing and the resulting colors are redder than observed SNe Ia (e.g., Kromer et al. 2010; Woosley & Kasen 2011; Polin et al. 2019; Collins et al. 2022). This can be alleviated in part by reducing the He shell mass, and, with bare sub- M_{Ch} CO WDs, good agreement with observations is found (e.g., Sim et al. 2010; Blondin et al. 2017; Shen et al. 2018a). With improved nucleosynthesis through the inclusion of a large nuclear network and CNO material in the He shell (Shen & Moore 2014), Townsley et al. 2019, Boos et al. 2021 and Shen et al. 2021 find that a thin He shell double detonation ($\lesssim 0.03 M_{\odot}$) can lead to good agreement with observations of spectroscopically normal SNe Ia (though their thin-shell results are at variance with Gronow et al. 2021; Collins et al. 2022).

The He detonation can be triggered by accretion stream instabilities during the dynamical phase of a double WD merger, with total accumulated He shell mass at ignition as low as $\approx 0.01 M_{\odot}$ (e.g., Guillochon et al. 2010; Pakmor et al. 2012). This dynamically driven double-degenerate double-detonation (D6) scenario is strongly supported by the discovery of three hyperve-

locity WDs with velocities $\gtrsim 1000 \text{ km s}^{-1}$ (Shen et al. 2018b).

Alternatively, the He detonation can arise during a He shell flash where the He shell accumulates through stable mass transfer. The donor can be a nondegenerate He star, with mass transfer rates $\approx 10^{-8} M_{\odot} \text{ yr}^{-1}$ leading to a thick He shell $\approx 0.1 - 0.2 M_{\odot}$ (e.g., Iben & Tutukov 1991; Brooks et al. 2015; Bauer et al. 2017), though the resulting transient better resembles peculiar SNe Ia (e.g., Woosley & Kasen 2011; Polin et al. 2019; De et al. 2019).

In the AM CVn last flash scenario, the donor is a cold He WD (Bildsten et al. 2007; Piersanti et al. 2015, 2019). The mass transfer rate begins high ($\dot{M} \gtrsim 10^{-6} M_{\odot} \text{ yr}^{-1}$), leading to weak He flashes, and decreases with time, leading to He flashes that increase in strength. The last He flash to occur is the strongest, and can potentially lead to a He detonation that results in a ‘‘Ia’’ supernova (Shen et al. 2010) or double-detonation SN Ia. However, Piersanti et al. (2015, 2019) suggest that the AM CVn last flash is not strong enough to become dynamical.

We revisit He WD donors as potential progenitors of double-detonations and hypervelocity WDs like D6-2. Motivated by the suggestion that AM CVn binaries can be born with a wide range of entropies (Deloye et al. 2007; Wong & Bildsten 2021; van Roestel et al. 2022; Burdge et al. 2023), we explore a binary scenario of stable mass transfer from a high-entropy (hot) He WD onto a massive CO WD that leads to a strong, first He flash potentially developing into a detonation of the He and possibly the CO.

We discuss the binary evolution models in Section 2. We show that high-entropy He WDs have lower peak \dot{M} than cold He WDs, leading to accretor He shell masses at ignition comparable to, or even greater than, in the AM CVn last flash scenario (Bildsten et al. 2007; Piersanti et al. 2015, 2019). In Section 3, we demonstrate that these He flashes can become dynamical and develop into a detonation, and discuss the minimum He shell mass required for such outcome. We show in Section 4 that high-entropy He WDs originate in binary scenarios from unstable mass transfer with an evolved $M = 1.3 - 2.0 M_{\odot}$ donor near the base of the red giant branch (RGB), and a short post common envelope (CE) orbital period. We conclude in Section 5 by discussing the open questions that remain.

2. BINARY EVOLUTION UP TO IGNITION OF THE HE SHELL

2.1. Setup

We model the mass transfer from a high-entropy He WD (donor) onto a CO WD (accretor) and the ensuing He flash on the accretor using Modules for Experiments in Stellar Astrophysics (MESA version 21.12.1; Paxton et al. 2011, 2013, 2015, 2018, 2019; Jermyn et al. 2023). The initial WD models are constructed in version 15140. Additional He flash models in Section 3.4 are run in version 22.11.1, chosen to test the new time dependent convection capability. Our MESA input and output files are available at Zenodo (<https://doi.org/10.5281/zenodo.7815303>).

We consider He WD donors with initial central entropies, $s_{\text{c,He}}^i / (N_{\text{A}} k_{\text{B}})$, where N_{A} is Avogadro’s constant and k_{B} is the Boltzmann constant, from 2.4 to 4.0 in increments of 0.1, and initial masses, M_{He}^i , from 0.15 to 0.25 M_{\odot} in increments of 0.01. We first evolve a 2.0 (for $M_{\text{He}}^i \leq 0.20 M_{\odot}$) or 2.5 M_{\odot} star from pre-main sequence to the formation of a He core of the desired mass (core boundary defined by hydrogen mass fraction $X = 10^{-5}$), with solar metallicity ($Z = 0.0142$; Asplund et al. 2009) and MESA’s `mesa_49.net` network, which includes neutrons, ^1H , ^3He , ^7Li , ^7Be , ^8B , ^{12}C , ^{13}C , ^{14}O , ^{17}F , ^{18}Ne , ^{21}Na , ^{23}Mg , ^{25}Al , ^{27}Si , ^{30}P , ^{31}S and interlinking reactions. Then we strip the envelope off using a fast wind with \dot{M} between 10^{-8} and $10^{-6} M_{\odot} \text{ yr}^{-1}$, and cool the He core to the desired central entropy.

We similarly construct CO WDs with initial masses, M_{WD}^i , of 0.9, 1.0 and 1.1 M_{\odot} . The 0.9 and 1.0 M_{\odot} models start with zero-age main sequence (ZAMS) masses of 5.5 and 6.3 M_{\odot} , and the 1.1 M_{\odot} model is scaled from the 1.0 M_{\odot} model after envelope stripping. The CO cores are cooled to a central temperature of $T_{\text{c}} = 2 \times 10^7 \text{ K}$. This range of CO masses is motivated by studies (e.g., Sim et al. 2010; Polin et al. 2019; Boos et al. 2021; Shen et al. 2021) that predict double detonations or bare CO detonations with CO cores in this mass range yield spectra and light curve evolution similar to subluminous, normal, and overluminous type Ia supernovae.

We initiate the WDs in a binary and evolve both components and orbital parameters. The initial orbital period is chosen such that the He WD comes into contact within 10^5 yr and its entropy then is the same as the initial value (see Section 4). We assume fully conservative mass transfer, modeled following Kolb & Ritter (1990), with orbital angular momentum loss driven solely by gravitational waves. For convergence, we set `eps_mdot_factor` = 0 for the donor. This neglects the redistribution of energy due to mass loss as laid out in Paxton et al. (2019), but has no effect on \dot{M} since it depends on the donor’s mass-radius relation (see Section 2.2).

We model both components as nonrotating. This could impact the stability of mass transfer, the mass transfer rate \dot{M} , and dissipation in the He shell of the accretor, all of which can influence the He shell thickness and thus strength of the He flash. However, as we explain here, we find any effects of rotation to be minimal. First, because of the larger radii of our high-entropy donors and the small mass ratio between the WDs, we find that disk accretion occurs for all runs in this study, using equation (6) of Nelemans et al. (2001), and so the mass transfer is stable (Marsh et al. 2004). Second, while a fully synchronized donor will be spun up to $\approx 30\%$ of critical rotation (e.g., Bauer & Kupfer 2021), we found that the resulting inflated radius is similar to that of a nonrotating model with slightly higher entropy ($\Delta s_{\text{c,He}}^i \approx 0.1$). The mass transfer rate is slightly lower, but we expect only a small shift in the parameter space for a strong He flash, by $\Delta s_{\text{c,He}}^i \approx 0.1$. Third, Neunteufel et al. (2017) found that while angular momentum transport by the Tayler-Spruit dynamo (Spruit 2002) can lead to near solid-body rotation in the accretor during accretion-induced spin-up, the resulting viscous dissipation can significantly reduce the required He shell mass for ignition. However, Piro (2008) found that viscous heating is unimportant compared to heating due to accretion for $\dot{M} \approx 10^{-7} M_{\odot} \text{ yr}^{-1}$ that is relevant for our work. Furthermore, we find that the enhanced Tayler-Spruit dynamo proposed by Fuller et al. (2019) reduces viscous dissipation even more considerably. Fourth, rotationally induced mixing between the CO core and He shell may impact ignition conditions. Studies considering hydrodynamic processes find considerable mixing. Yoon et al. (2004) find that mixing tends to stabilize He burning, while Piro (2015) finds that mixing occurs earlier but at a larger depth. In contrast, Neunteufel et al. (2017), who consider the Tayler-Spruit dynamo, find little mixing at the core-shell interface. Finally, tidal dissipation may also reduce the required He shell mass for ignition (see Fuller & Lai 2012, for the hydrogen, non-accreting counterpart). We defer to future studies for investigating this possibility.

During the binary run, we adopt a nuclear network that includes ^{14}C , since it participates in the $^{14}\text{N}(e^-, \nu)^{14}\text{C}(\alpha, \gamma)^{18}\text{O}$ (NCO) reaction chain (Hashimoto et al. 1986) at densities above $1.25 \times 10^6 \text{ g cm}^{-3}$, and may trigger an earlier ignition for thick He shells (Bauer et al. 2017). We calculate the weak reaction rates linking ^{14}N and ^{14}C following Schwab et al. (2017), which agree within 50% for $5.5 \leq \log_{10}(Y_e \rho / \text{g cm}^{-3}) \leq 7.0$ where $Y_e = 0.5$, and $7.0 \leq \log_{10}(T/\text{K}) \leq 8.3$ with the rates provided by G. Martínez-Pinedo in the MESA custom_rates test suite, but

are more finely spaced in $\log_{10} \rho$ space and so avoids interpolation issues when the rates change by orders of magnitude. The $^{14}\text{C}(\alpha, \gamma)^{18}\text{O}$ rates are from Bauer et al. (2017).

We assume that a phase of H-rich mass transfer has already occurred prior to the He-rich phase modeled in this work (e.g., extremely low-mass WDs are expected to have $\approx 10^{-3} M_{\odot}$ of H on their surface; Istrate et al. 2016). The H-rich mass transfer causes H flashes on the accretor, and given the short binary separation, the accretor may expand and fill its own Roche-lobe. We assume that the binary survives the H-novae by ejecting the H shells, as is found likely for a $0.2 + 1.0 M_{\odot}$ binary in Shen (2015).

As He-rich mass transfer begins, the temperature in the accretor envelope rises due to compression, forming a temperature inversion, and eventually reaches ignition. We terminate the binary run once a convection zone is formed, and continue evolving the accretor through the He flash until the convection zone reaches the surface. This will be described in more detail in Section 3.

2.2. Mass transfer history

High-entropy He WD donors yield a lower \dot{M} , and, when thermally unstable, a thicker He shell at ignition than a cold He WD donor (Deloye et al. 2007). By high-entropy, we mean the He WD is hotter and less dense, and has a lower degree of degeneracy. For this study, we consider He WDs with central entropy $s_{\text{c,He}}/(N_{\text{A}} k_{\text{B}}) \gtrsim 3.0$ high-entropy, corresponding to a cooling time $\lesssim 10^8 \text{ yr}$ after their formation (see Section 4). With their larger radii, high-entropy He WDs reach period minimum and peak \dot{M} at longer P_{orb} , where they have longer gravitational wave timescales, $\tau_{\text{gr}} \equiv J_{\text{orb}}/\dot{J}_{\text{gr}}$ where J_{orb} is the orbital angular momentum and \dot{J}_{gr} is the rate of angular momentum loss due to gravitational wave radiation (Landau & Lifshitz 1971). The timescale for orbital evolution is given by τ_{gr} , and $\dot{M} \approx M_{\text{He}}/\tau_{\text{gr}}$ (e.g., Bauer & Kupfer 2021). Therefore, high-entropy He WDs have lower peak \dot{M} , as a consequence of their larger radii. There is a donor entropy so large that the low \dot{M} leads to accumulation of a He layer that never undergoes a flash.

Figure 1 compares the mass transfer histories for He WD donors with $M_{\text{He}}^i = 0.15, 0.20 M_{\odot}$, $M_{\text{WD}}^i = 1.0 M_{\odot}$, and a wide range of $s_{\text{c,He}}^i$. It illustrates that a higher-entropy He WD has a lower peak \dot{M} and a longer period minimum. Higher-entropy He WDs also start with a thicker nondegenerate layer on the surface, and so come into contact at longer P_{orb} . Removal of the nondegenerate layer leads to contraction of the radius (Deloye et al. 2007; Kaplan et al. 2012), so P_{orb} de-

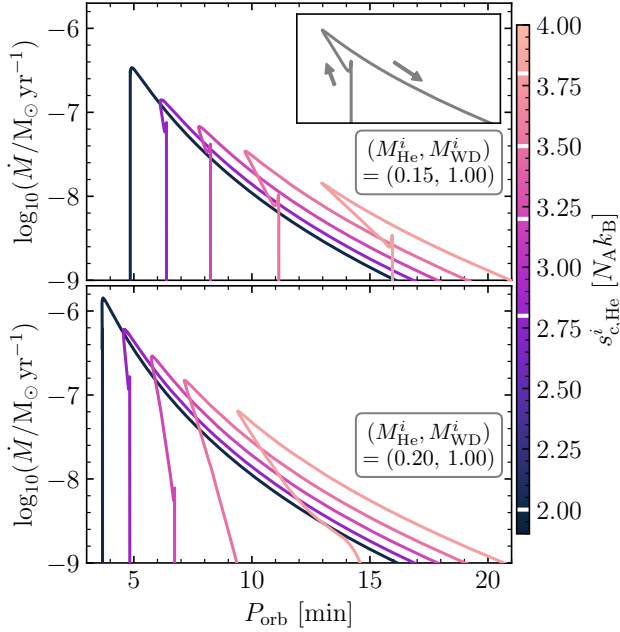


Figure 1. Mass transfer rate, \dot{M} , as a function of orbital period, P_{orb} , for He WDs with $M_{\text{He}}^i = 0.15$ (top) or $0.20 M_{\odot}$ (bottom) of various $s_{\text{c,He}}^i$ transferring mass onto a $M_{\text{WD}}^i = 1.0 M_{\odot}$ accretor. Inset indicates the flow of time.

creases and \dot{M} gradually increases from $\lesssim 10^{-8} M_{\odot} \text{ yr}^{-1}$ to $\approx 10^{-7} M_{\odot} \text{ yr}^{-1}$. This is seen in the high-entropy models in the “turn-on” phase of mass transfer. Moreover, comparison between the top and bottom panels shows that for higher M_{He}^i , the period minimum occurs at shorter P_{orb} , and peak \dot{M} is higher, at fixed $s_{\text{c,He}}^i$. This is a consequence of their smaller radii. However, the \dot{M} evolution is eventually the same regardless of M_{He}^i , for the models with the same $s_{\text{c,He}}^i$ (Deloye et al. 2007; Wong & Bildsten 2021).

We do not consider initial entropies higher than $s_{\text{c,He}}^i / (N_{\text{A}} k_{\text{B}}) = 4.0$. He WDs with initial entropies below roughly this value have high enough \dot{M} that the mass transfer timescale, $\tau_{\dot{M}} \equiv M_{\text{He}} / \dot{M}$, is shorter than the thermal timescale, $\tau_{\text{th}} \equiv \int_0^{M_{\text{He}}} (c_{\text{p}} T dm) / L_{\text{He}}$, leading to adiabatic evolution (Deloye et al. 2007; Wong & Bildsten 2021). With $s_{\text{c,He}}^i / (N_{\text{A}} k_{\text{B}}) \gtrsim 4.0$, \dot{M} during the “turn-on” phase is so low that $\tau_{\dot{M}} > \tau_{\text{th}}$. The donor therefore loses entropy until $s_{\text{c,He}} / (N_{\text{A}} k_{\text{B}})$ decreases down to ≈ 4.0 , where $\tau_{\dot{M}} \lesssim \tau_{\text{th}}$ and adiabatic evolution begins. As a result, all He WDs with $s_{\text{c,He}}^i / (N_{\text{A}} k_{\text{B}}) \gtrsim 4.0$ eventually resemble a $s_{\text{c,He}}^i / (N_{\text{A}} k_{\text{B}}) \approx 4.0$ one in \dot{M} evolution.

2.3. Properties at Onset of He Flash

Panels (a) and (e) of Figure 2 show properties of the accretor and donor that are determined at He shell ignition, for our fiducial grid of $M_{\text{WD}}^i = 1.0 M_{\odot}$ models. Similar results are shown in Figure 3 for $M_{\text{WD}}^i = 0.9, 1.1 M_{\odot}$ models.

The total accumulated He shell masses at ignition (panel a) of our models span the range of $0.01 - 0.08 M_{\odot}$. These cover the range of He shell masses predicted by Bildsten et al. (2007) and Piersanti et al. (2015) for the AM CVn last flash scenario. Three trends can be observed. First, with a higher $s_{\text{c,He}}^i$ at fixed M_{He}^i , a thicker He shell is required for ignition. This is the result of less efficient “compressional heating” due to the lower \dot{M} . The thickest He shells here are ignited with a boost from the NCO reaction chain occurring near the base of the accreted layer (Hashimoto et al. 1986; Bauer et al. 2017). Second, no He flash occurs above a certain $s_{\text{c,He}}^i$ for each M_{He}^i , due to the very low \dot{M} for these models. These systems will continue to evolve as an AM CVn binary to long orbital periods (e.g., Ramsay et al. 2018; Wong & Bildsten 2021), possibly explaining why some AM CVn donors have high-entropy (van Roestel et al. 2022). Third, the parameter space for the same range of ΔM shifts to higher $s_{\text{c,He}}^i$ as M_{He}^i increases. This is because ΔM largely depends on peak \dot{M} , which is higher as M_{He}^i increases, and lower as $s_{\text{c,He}}^i$ increases.

While it is unclear whether all these models can develop a He detonation, they do support a steady transverse detonation wave, especially given the inclusion of a large nuclear network and modest enrichment of CNO material (Shen & Moore 2014). If double-detonation is successful, the ones with $\Delta M \lesssim 0.03 M_{\odot}$ are of interest for spectroscopically normal type Ia supernovae, while models with thicker He shells may resemble abnormal thermonuclear supernovae (Polin et al. 2019; Boos et al. 2021).

Following (if possible) the double-detonation of the accretor and the unbinding of the binary, the donor departs at its pre-explosion orbital velocity, which is shown in panel (e) of Figure 2. The radius of the donor, and hence P_{orb} at period minimum, increase with $s_{\text{c,He}}^i$, leading to a decrease of $v_{\text{orb,He}}^{\text{ign}}$ with $s_{\text{c,He}}^i$. Typical low-entropy ($s_{\text{c,He}}^i / (N_{\text{A}} k_{\text{B}}) \lesssim 3.0$) donors have $v_{\text{orb,He}}^{\text{ign}} \gtrsim 1100 \text{ km s}^{-1}$, but high-entropy donors may reach $v_{\text{orb,He}}^{\text{ign}} \approx 1000 \text{ km s}^{-1}$, becoming comparable to the heliocentric velocity of the hypervelocity WD D6-2 ($1010_{-50}^{+60} \text{ km s}^{-1}$; Bauer et al. 2021). A lower M_{WD}^i gives a lower $v_{\text{orb,He}}^{\text{ign}}$ at fixed $s_{\text{c,He}}^i$ (though the boundary for ignition may change slightly), by $\approx 40 - 50 \text{ km s}^{-1}$ for $M_{\text{WD}}^i = 0.9 M_{\odot}$ (see Figure 3), allowing for a larger parameter space for matching D6-2. Regardless of M_{WD}^i ,

our models confirm the analysis by Bauer et al. (2021) that D6-2 could be a former He WD donor¹ where a double-detonation may have happened, and our results furthermore suggest that D6-2 must have been high-entropy.

3. THE HE SHELL FLASH

Important parameters adopted during the He flash are as follows. First, the accretor’s nuclear network is expanded to include neutrons, ^1H , ^4He , ^{11}B , $^{12-14}\text{C}$, $^{13-15}\text{N}$, $^{14-18}\text{O}$, $^{17-19}\text{F}$, $^{18-22}\text{Ne}$, $^{21-23}\text{Na}$, $^{22-26}\text{Mg}$, $^{25-27}\text{Al}$, $^{27-30}\text{Si}$, $^{29-31}\text{P}$, $^{31-34}\text{S}$, $^{33-35}\text{Cl}$, $^{36-39}\text{Ar}$, ^{39}K , ^{40}Ca , ^{43}Sc , ^{44}Ti , ^{47}V , ^{48}Cr , ^{51}Mn , $^{52,56}\text{Fe}$, ^{55}Co , and $^{55,56,58-59}\text{Ni}$. This gives a network that encompasses the 55-isotope network adopted by Townsley et al. (2019) for accurate energy release. In particular, the reaction $^{12}\text{C}(p, \gamma)^{13}\text{N}(\alpha, p)^{16}\text{O}$ yields significant energy release at temperatures above 10^9K (Shen & Bildsten 2009; Shen & Moore 2014), and plays an important role in some of our models. Second, we adopt the Cox formulation of the mixing length theory (MLT; Cox & Giuli 1968), and a mixing length parameter $\alpha_{\text{MLT}} = 2$. We adopt the Ledoux criterion, and include semiconvective mixing (with an efficiency $\alpha_{\text{semi}} = 1$; Langer et al. 1985) and thermohaline mixing (with an efficiency of 1; Brown et al. 2013). Third, we relax the tolerances to

```
gold2_tol_residual_norm3 = 1d-6
gold2_tol_max_residual3 = 1d-3 ,
```

and upon two consecutive retries, we temporarily set `use_dPrad_dm_form_of_T_gradient_eqn = .true.`² which often aids solver convergence, particularly at the top boundary of the convection zone.

3.1. Fiducial grid

Due to heat transport away from the temperature peak during the He shell’s accumulation, ignition occurs above the base of the accreted layer by $\approx 0.004 - 0.025 M_{\odot}$. This is illustrated by panel (b) of Figure 2, which shows the mass exterior to the base of the convection zone (BCZ) at $\log_{10}(T_{\text{bcz}}/\text{K}) \gtrsim 8.3$. This is slightly larger than when the convection zone first appears, because initially the inner convective boundary moves inwards until $\log_{10}(T_{\text{bcz}}/\text{K}) \gtrsim 8.3$. We do not include mixing beyond the convective boundary via overshooting, nor the convective premixing or predictive mixing schemes for determining the convective boundary (e.g.,

¹ Alternatively, D6-2 could be a former He star donor (Neunteufel et al. 2021), or former CO WD accretor with a hybrid He/CO donor (Pakmor et al. 2021).

² <https://docs.mesastar.org/en/release-r22.05.1/reference/controls.html#use-dprad-dm-form-of-t-gradient-eqn>

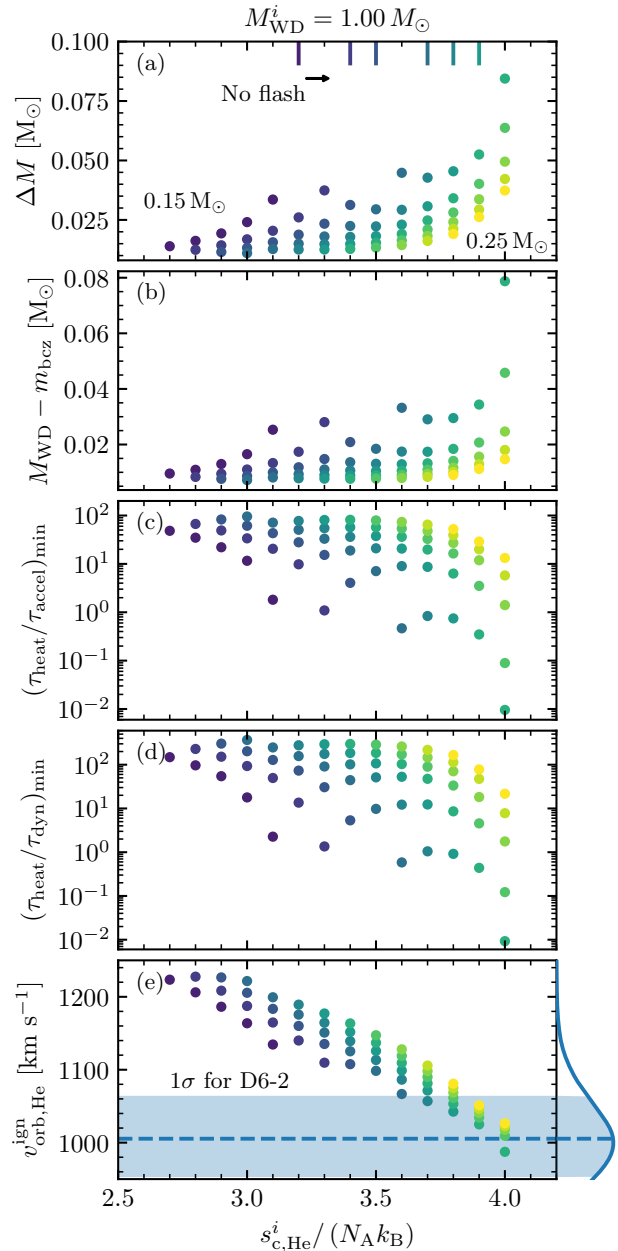


Figure 2. Total accumulated He shell mass at ignition, mass exterior to the base of the convection zone (BCZ), minimum $\tau_{\text{heat}}/\tau_{\text{accel}}$ where convective velocity is greatest, $\tau_{\text{heat}}/\tau_{\text{dyn}}$ at the BCZ, and the orbital velocity of the donor at the start of the He flash, from top to bottom. All runs start with $M_{\text{WD}}^i = 1.0 M_{\odot}$, and color-coding indicates M_{He}^i , from $0.15 M_{\odot}$ for the darkest color, to $0.25 M_{\odot}$ for the lightest color. For each M_{He}^i set, we indicate the minimum $s_{\text{c,He}}^i$ above which no He flash occurs, by the lines at the top of the first panel. In the bottom panel, we show the heliocentric velocity of the hypervelocity WD D6-2 (dash-blue line) with its 1σ uncertainty (blue region). Its posterior probability distribution (Bauer et al. 2021) is shown on the side.

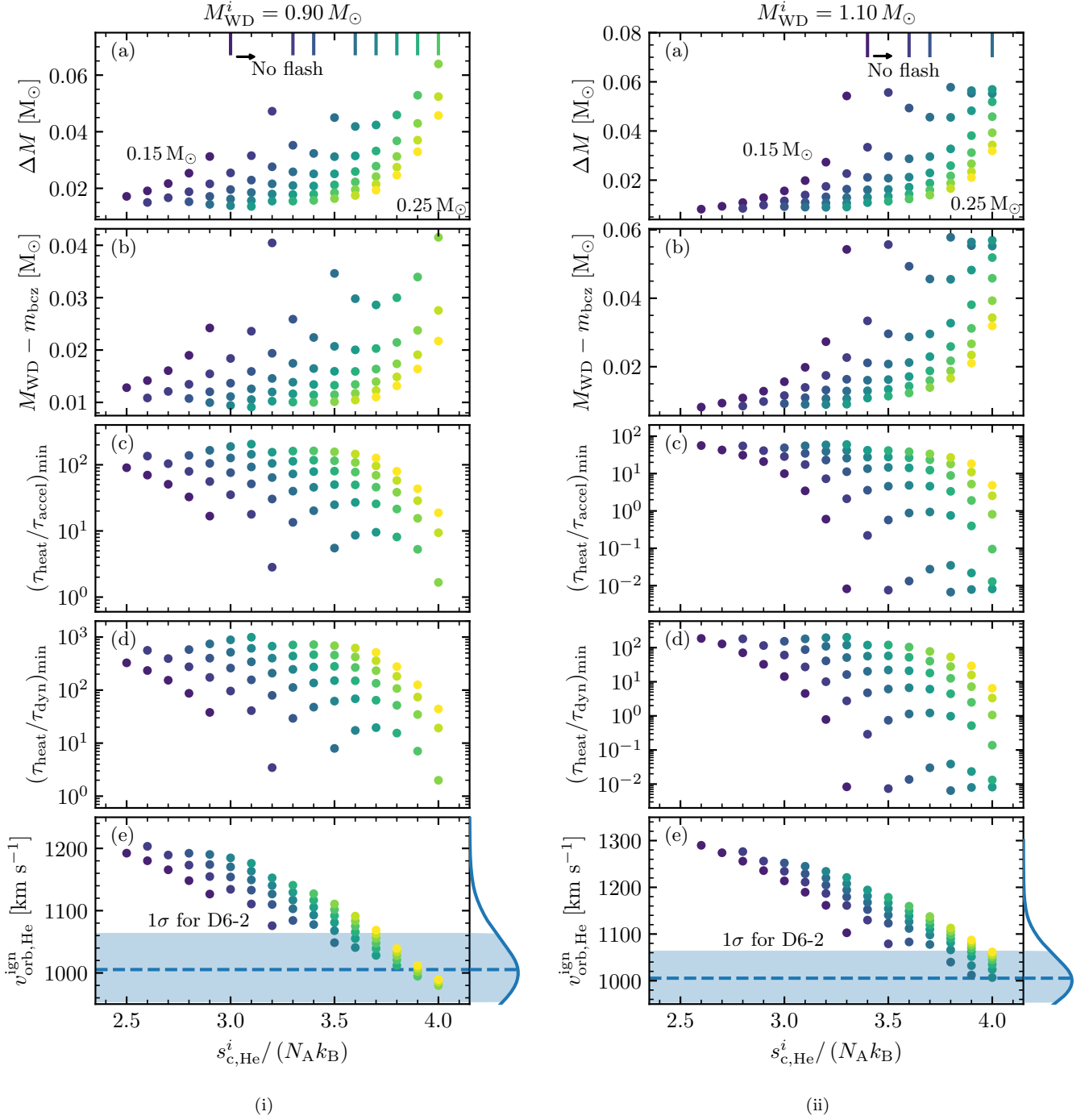


Figure 3. Same as Figure 2, but with $M_{\text{WD}}^i = 0.9, 1.1 M_{\odot}$ for the left and right panels respectively.

Paxton et al. 2018, 2019). However, any mixing beyond the convective boundary would move the BCZ further inwards, creating a more explosive outcome. In Section 3.4, we artificially induce ignition at the base of the accreted layer. Furthermore, in Section 3.3 we show the effects of adopting a different accretor T_c and conductive opacity, both of which influence conditions at the BCZ.

Three timescales affect the outcome of the He flash. The first is the dynamical timescale,

$$\tau_{\text{dyn}} = \frac{H}{c_s}, \quad (1)$$

where H is the pressure scale height and c_s is the sound speed. The second is the local heating timescale, at which temperature increases due to burning,

$$\tau_{\text{heat}} = \frac{c_p T}{\epsilon_{\text{nuc}}}, \quad (2)$$

where c_p is the specific heat capacity and ϵ_{nuc} is the nuclear energy generation rate. This is smaller than the global heating timescale over the convective envelope, $\tau_{\text{heat,global}} = \int (c_p T dm) / \int (\epsilon_{\text{nuc}} dm)$, which is the time to heat the entire convection zone (Shen & Bildsten 2009). The third is the convective acceleration timescale, at which convective velocity, v_c , varies (Jermyn et al. 2023) and which is given by, in MESA default parameters,

$$\tau_{\text{accel}} = \frac{3H}{\sqrt{2c_p T \nabla_a (\nabla - \nabla_L)}}, \quad (3)$$

where ∇ is the temperature gradient, ∇_a is the adiabatic gradient, and ∇_L is the Ledoux gradient. In steady state, τ_{accel} is $3/(2\alpha_{\text{MLT}})$ times the eddy turnover timescale,

$$\tau_{\text{eddy}} = \frac{H}{v_c}. \quad (4)$$

When $\tau_{\text{heat}} \lesssim \tau_{\text{accel}}$, the standard assumption that convection is in steady state becomes dubious, since the temperature rises faster than convection can respond. Instead, convection is expected to freeze out (e.g., Woosley & Kasen 2011; Jermyn et al. 2023). When time-dependent convection (TDC) is applied, heat is more strongly trapped at the BCZ, leading to strong superadiabaticity and a higher peak T_{bcz} (see Jermyn et al. 2023). Woosley & Weaver (1994) also argue that convection breaks down when $\tau_{\text{heat}} \lesssim \tau_{\text{eddy}}$. A subsonic, turbulence-dominated deflagration results and, although not well-studied for He, may transition into a detonation (e.g., Shen et al. 2010).

When $\tau_{\text{heat}} \lesssim \tau_{\text{dyn}}$ locally, an overpressure develops over the scale height and a detonation is very likely. Moreover, Shen & Moore (2014) show that, if a large

nuclear net and CNO isotopes are included, the detonation may well initiate in a hotspot that is small (required to be at least $\approx 3 \times 10^6$ cm for an isobaric hotspot with central temperature 10^9 K and central density 10^5 g cm $^{-3}$) compared to the scale height of the convection zone (\approx few $10^7 - 10^8$ cm). In this case, the local heating timescale should be compared to the sound-crossing time over the dimension of the hotspot, which makes a detonation even more likely (Shen & Moore 2014). In addition, many He flashes realized in this work are ignited above the base of the accreted layer and mixing beyond the convective boundary can induce a stronger He flash. For these two reasons, we consider $\tau_{\text{heat}} \lesssim 100 \tau_{\text{dyn}}$ of interest, as long as the envelope can sustain a steady transverse detonation wave. We note that a hydrodynamical approach is more appropriate in the limit $\tau_{\text{heat}} \lesssim \tau_{\text{dyn}}$, as is done by Woosley & Kasen (2011) in 1D, but we continue to adopt a hydrostatic approach for numerical convenience and to approximate $\tau_{\text{heat}}/\tau_{\text{dyn}}$ of our models. Furthermore, when $\tau_{\text{heat}} \approx \tau_{\text{dyn}}$, τ_{heat} already approaches ≈ 0.1 times $\pi r_{\text{bcz}}/c_s$, i.e., the time for sound waves to communicate over a shell of radius r_{bcz} . In other words, multiple points at the BCZ may initiate an ignition (e.g., Woosley & Kasen 2011). Future three-dimensional simulations similar to Zingale et al. (2013), Jacobs et al. (2016), and Glasner et al. (2018) may further inform the exact conditions of the initiation of a detonation.

The minimum values of the ratios $\tau_{\text{heat}}/\tau_{\text{accel}}$ and $\tau_{\text{heat}}/\tau_{\text{dyn}}$ are compared in panels (c) and (d) of Figure 2. A thicker He shell leads to a higher P_{bcz} for hydrostatic balance, and a higher peak T_{bcz} . These both lead to stronger nuclear burning, and hence lower τ_{heat} . Therefore, $\tau_{\text{heat}}/\tau_{\text{accel}}$ and $\tau_{\text{heat}}/\tau_{\text{dyn}}$ both decrease with ΔM , and hence $s_{c,\text{He}}^i$. Some of our models, with total accumulated He masses of $\gtrsim 0.03 M_\odot$, can reach $\tau_{\text{heat}}/\tau_{\text{dyn}} \lesssim 10$. This suggests that high-entropy He WD are a viable channel for He detonations and related transients.

3.2. Different accretor mass

In Figure 3, we show the results for an initially $M_{\text{WD}}^i = 0.9, 1.1 M_\odot$ accretor. Both show a similar range of total accumulated He shell mass at ignition as the fiducial $1.0 M_\odot$ grid, but as M_{WD}^i increases, the minimum ratio between τ_{heat} and τ_{dyn} , and τ_{heat} and τ_{accel} decrease. This results from the increasing density at the He base as M_{WD}^i increases. As M_{WD}^i increases, so does the surface gravity and density at the base of the He shell. As a result, for the same M_{He}^i and $s_{c,\text{He}}^i$, the total accumulated He shell mass at ignition, minimum ratio between τ_{heat} and τ_{dyn} , and τ_{heat} and τ_{accel} , decrease

with M_{WD}^i . In other words, for a given M_{He}^i , in order to achieve a dynamical He flash, a higher M_{WD}^i requires a slightly lower $s_{\text{c,He}}^i$. Also due to the increasing density at the He shell base with M_{WD}^i , none of the $0.9 M_{\odot}$ models show ignition boosted by the NCO reaction chain, but highest entropy models with $M_{\text{WD}}^i = 1.0, 1.1 M_{\odot}$ do, as the density at the He base reaches the critical density $1.25 \times 10^6 \text{ g cm}^{-3}$ (Bauer et al. 2017).

3.3. Other variables

In this work we include the correction by Blouin et al. (2020) to the electron conductive opacities, which results in a lower opacity in the He envelope of the accretor. Due to the faster transport of heat away from the envelope, a higher He shell mass is required for ignition. However, the Blouin et al. (2020) correction, while accurate at moderate degeneracy, may not be appropriate at strong degeneracy (Cassisi et al. 2021). We re-ran our $M_{\text{He}}^i = 0.15 M_{\odot}$, $s_{\text{c,He}}^i/(N_{\text{A}}k_{\text{B}}) = 3.1$ binary applying the damping factors proposed by Cassisi et al. (2021) to the accretor. With a ‘weak (strong) damping’, the total accumulated He mass at ignition is reduced from $0.034 M_{\odot}$ to $0.032(0.027) M_{\odot}$, while the mass enclosed by the BCZ is increased from $1.008 M_{\odot}$ to $1.012(1.012) M_{\odot}$. Both result in a slightly weaker He flash, with the minimum $\tau_{\text{heat}}/\tau_{\text{dyn}}$ increased from 2.2 to 6.5(23.8). Nevertheless, the uncertainty in the electron conductive opacities plays a minor role in our simulations, compared to, e.g., the mass transfer history.

While we fix the initial center temperature of the accretor to $T_{\text{c}} = 2 \times 10^7 \text{ K}$, we test the effects of different choices of T_{c} by re-running the $M_{\text{He}}^i = 0.15 M_{\odot}$, $s_{\text{c,He}}^i/(N_{\text{A}}k_{\text{B}}) = 3.0$ binary. The fiducial run has a total accumulated He mass of $0.024 M_{\odot}$ and a mass enclosed by the BCZ of $1.008 M_{\odot}$, which are changed to $0.027, 0.022, 0.019 M_{\odot}$ and $1.010, 1.005, 1.002 M_{\odot}$ for $\log_{10}(T_{\text{c}}/\text{K}) = 7.0, 7.5, 7.7$ respectively. In other words, a hotter initial accretor results in a lower accumulated He mass at ignition and ignition closer to the center (e.g., Woosley & Kasen 2011). These opposing effects largely cancel and result in a similar minimum $\tau_{\text{heat}}/\tau_{\text{dyn}}$, with 17.9 for the fiducial and 15.5, 19.8, and 22.3 for $\log_{10}(T_{\text{c}}/\text{K}) = 7.0, 7.5, 7.7$ respectively.

3.4. Envelope mass condition for dynamical flash

Our models differ from those in Shen & Bildsten (2009) because ours allow superadiabaticity in the convective zone and use a large nuclear net. We now explore the impacts of these two choices on the envelope mass required for a dynamical flash.

We construct He flash models with different combinations of core mass M_{core} and envelope mass M_{env} as

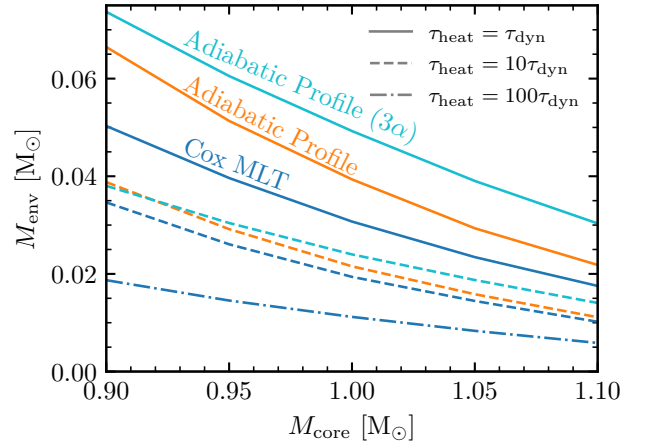


Figure 4. He envelope mass required such that $\tau_{\text{dyn}}/\tau_{\text{heat}}$ at the BCZ reaches 1 (solid lines), 10 (dashed lines), and 100 (dot-dashed; only for Cox MLT) for a given mass enclosed by the BCZ. Dark blue, orange and light blue lines correspond to Cox MLT, adiabatic profile, and adiabatic profile with only triple-alpha burning.

follows. We first scale the $1.0 M_{\odot}$ CO WD ($X(^{16}\text{O}) \approx 0.61, X(^{12}\text{C}) \approx 0.37, X(^{22}\text{Ne}) \approx 0.02$) to the desired M_{core} . Then we accrete material similar in composition to the $0.15 M_{\odot}$ He WD ($X(^4\text{He}) \approx 0.986, X(^{14}\text{N}) \approx 0.0088$, where the progenitor star has $Z = 0.0142$), onto the CO WD until M_{env} is reached, at $\dot{M} = 10^{-8} M_{\odot} \text{ yr}^{-1}$ so that the He does not ignite. The CO WD is allowed to cool until $T_{\text{c}} = 2 \times 10^7 \text{ K}$. Finally, the envelope is artificially heated at its base until a convection zone appears. In other words, unlike in the binary evolution, the BCZ is located at the base of the accreted material.

We run grids of models with 3 different treatments of convection: (1) with Cox MLT allowing superadiabaticity, which is the same as in Section 3.1; (2) forcing an adiabatic profile in the convection zone; and (3) forcing an adiabatic profile, accounting for only the triple-alpha reaction and not allowing compositional changes so as to simulate a nearly pure He envelope, as is assumed in Shen & Bildsten (2009). Adiabatic convection is enforced by the MLT++ capacity (Paxton et al. 2013), via the MESA controls:

```
okay_to_reduce_gradT_excess = .true.
gradT_excess_lambda1 = -1
gradT_excess_max_logT = 12 ,
```

which, together, ensure that superadiabaticity in the convection zone is fully reduced.

From the grids of models, we interpolate in M_{core} and M_{env} to find where $\tau_{\text{heat}} = \tau_{\text{dyn}}$, $\tau_{\text{heat}} = 10\tau_{\text{dyn}}$, and $\tau_{\text{heat}} = 100\tau_{\text{dyn}}$ (for Cox MLT only). These are

shown in Figure 4. For a given M_{core} , the adiabatic profile with only triple-alpha burning requires the thickest M_{env} , followed in order by the adiabatic profile and Cox MLT. The difference between the first two reflects the importance of including a large nuclear net, in particular the reaction $^{12}\text{C}(p, \gamma)^{13}\text{N}(\alpha, p)^{16}\text{O}$ (Shen & Bildsten 2009; Shen & Moore 2014), though this is slightly metallicity-dependent since the protons are produced from reactions like $^{14}\text{N}(\alpha, \gamma)^{18}\text{F}(\alpha, p)^{21}\text{Ne}$ (Shen & Bildsten 2009). However, we varied the metallicity of the $M_{\text{core}} = 1.0 M_{\odot}$, $\log_{10}(M_{\text{env}}/M_{\odot}) = -1.5$ model, and found that the minimum $\tau_{\text{heat}}/\tau_{\text{dyn}}$ changes from 1.45 at $0.1 Z_{\odot}$, to 0.86 at Z_{\odot} (our fiducial), and to 0.77 at $2 Z_{\odot}$, so the uncertainty resulting from varying metallicity plays a small role. The difference between the adiabatic profile and Cox MLT arises because, for a given M_{core} and M_{env} , superadiabaticity as allowed by Cox MLT results in a higher peak T_{bcz} , which in turn reduces τ_{heat} . Finally, we further run a grid of models with TDC (again allowing superadiabaticity), which agrees well with Cox MLT for less dynamical flashes. With more dynamical flashes, because the inequality $\tau_{\text{heat}} \lesssim \tau_{\text{accel}}$ strengthens, TDC exhibits stronger heat-trapping at the BCZ (see Section 3.6 of Jermyn et al. 2023, for more details). This results in a larger superadiabaticity and a larger peak T_{bcz} . However, the reduction in M_{env} required for $\tau_{\text{heat}} = \tau_{\text{dyn}}$ is $\lesssim 5\%$.

In agreement with Woosley & Kasen (2011), we find that the $^{12}\text{C}(p, \gamma)^{13}\text{N}(\alpha, p)^{16}\text{O}$ reaction reduces the minimum M_{env} required for a dynamical He flash. Our Cox MLT, $\tau_{\text{heat}} = \tau_{\text{dyn}}$ line agrees well with their “hot” line (see their Figure 19) at $M_{\text{core}} \approx 0.9 M_{\odot}$, but is slightly lower by $\approx 30\%$ at $\approx 1.1 M_{\odot}$. The reason could be that they define τ_{heat} as the time to run away to 1.2×10^9 K and they have a sparser grid of models.

4. HOW TO MAKE HIGH-ENTROPY HE WDS?

Now the question is, how does one obtain He WDs that are high-entropy at contact? We address this first assuming that the He WD is formed through a CE event.

First, the He WD has to be high-entropy at formation. Figure 5 shows the evolution on the HR diagram of stars of $M = 1.0 - 2.5 M_{\odot}$ (without mass loss), from the start of core H burning through the RGB. Contours label s_c and M_{He} (where the He core boundary is defined by H mass fraction $X = 0.1$ in this section) in the left and right panels respectively. As the He core mass grows while the star crosses the Hertzsprung gap (HG) and ascends the RGB, s_c drops. With higher MS progenitor mass, a given M_{He} is formed earlier with higher s_c . As the CE event happens on short timescales, s_c of the post-CE He WD is the same as that of the pre-CE

He core. Thus, if a CE event occurs early in the post-MS evolution (near the base of the RGB)³, corresponding to an orbital period of $\approx 1 - 8$ d for a $1.0 M_{\odot}$ companion, then a high-entropy He WD can be obtained at formation.

Second, this high-entropy He WD should not cool before coming into contact. Figure 6 shows the cooling evolution of He WDs of various masses, in central temperature and density space. Comparison between the lines of constant s_c and those of constant cooling age, shows that the high entropies required by our scenario, $s_c/(N_A k_B) = 3.0 - 4.0$, implies that the He WDs can only cool for $\lesssim 10^8$ yr between their formation and the onset of He mass transfer.

Third, in order to have cooled for little time before contact, the binary has to be formed at short orbital periods. For example, the gravitational-wave-induced merger timescale, which can be taken as the time before the binary comes into contact again, is $\approx 10^8$ yr for a $0.2 M_{\odot} + 1.0 M_{\odot}$ binary with an orbital period of ≈ 1 hr.

Such short post-CE periods are favored by recent findings that the CE efficiency is low (e.g., Zorotovic et al. 2010; Scherbak & Fuller 2023), as well as suggestions that ELM WDs are formed at short orbital periods (Brown et al. 2016). Along each evolutionary track in Figure 5, we assume that the He WD progenitor (star 1) fills its Roche lobe and undergoes a CE event, during which the companion (star 2) remains at the same mass. Assuming that the change in orbital energy during the CE event is used to eject the CE with an efficiency of $\alpha \approx 1/3$ (e.g., Scherbak & Fuller 2023), we solve the CE energy equation for the post-CE binary separation, a_f ,

$$E_{\text{bind}} = \alpha \left(\frac{GM_1 M_2}{2a_i} - \frac{GM_{\text{He}} M_2}{2a_f} \right), \quad (5)$$

where E_{bind} is the binding energy of the envelope obtained from MESA accounting for recombination energy, and the pre-CE binary separation, a_i , is given by the RLOF condition for star 1 (Eggleton 1983)

$$a_i = R_1 \frac{0.6q_1^{2/3} + \ln(1 + q_1^{1/3})}{0.49q_1^{2/3}}, \quad (6)$$

where $q_1 = M_1/M_2$.

A low CE parameter e.g., $\alpha = 1/3$ favors formation of He WD binaries at ultrashort periods $P_{\text{orb}} \ll 1$ hr, which have very short gravitational wave merger timescales.

³ We assume a CE event will happen since the RGB star has a deep convective envelope ($q_{\text{conv}} \gtrsim 0.5$). For more realistic conditions, see, for example, Temmink et al. (2023).

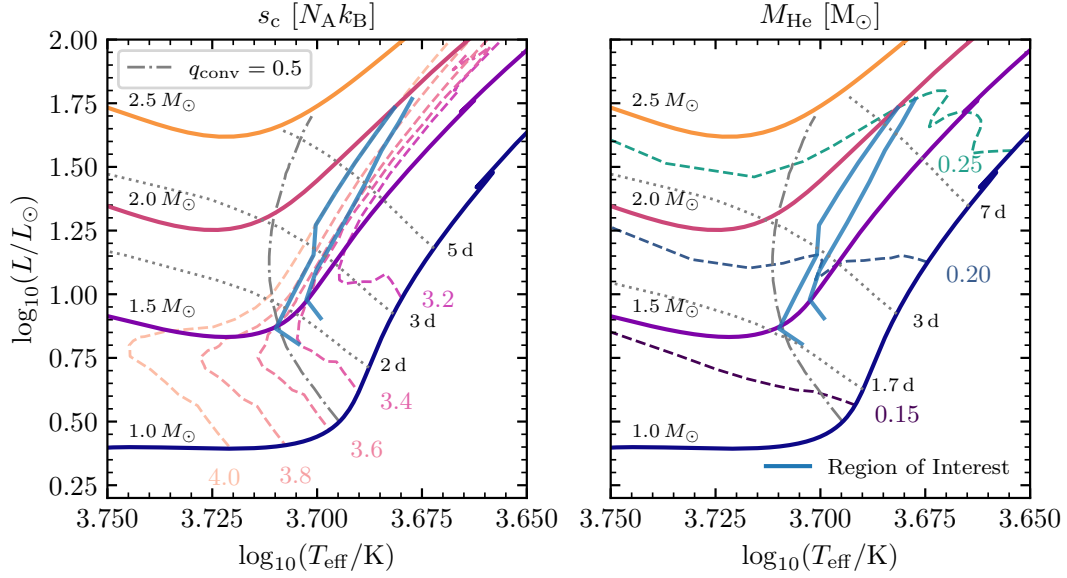


Figure 5. Evolution of $1.0 - 2.5 M_{\odot}$ stars up the RGB, with contours labeling central specific entropy (left) and He core mass (right). The two blue lines bracket parameter space for which a dynamical He flash may happen once mass transfer occurs after the CE event. The convective envelope occupies half of the star’s total mass to the right of the dot-dashed line. The three dotted lines label the orbital periods of 2, 3, 5 days (left), and 1.7, 3, 7 days (right) where the star fills its Roche lobe with a $1.0 M_{\odot}$ companion.

For systems with $M_{\text{He}} \gtrsim 0.25 M_{\odot}$ and $M \lesssim 1.5 M_{\odot}$, there is sufficient time for the newly formed He WD to cool, but they do not lead to dynamical flashes. In contrast, systems that do lead to dynamical flashes, marked as the region of interest in Figure 5, will remain at the same entropy. However, the post-CE binary may be so compact that the newly-formed He WD immediately fills its Roche lobe (e.g., Deloye et al. 2007). We remain agnostic as to whether this leads to a merger outcome or that a transition to stable mass transfer is possible. If the latter case does occur, our work suggests that a CE event occurring at the base of the RGB favors the formation of a high-entropy He WD donor amenable to a dynamical He flash from later mass transfer.

In the stable mass transfer channel for ELM WD formation, a pre-ELM WD with mass $\gtrsim 0.15 M_{\odot}$ becomes detached at $P_{\text{orb}} \gtrsim 5$ hr (e.g., Sun & Arras 2018). Although these models have thick H shells and undergo stable H burning which maintains a warm He core (Kaplan et al. 2012), the He WD will still have cooled for too long and become low-entropy before coming into contact again. This is shown by the grey dots in Figure 6, where the models are made following Sun & Arras (2018). Given this, we suggest that a high-entropy He WD has to descend from the CE channel with a short post-CE orbital period $P_{\text{orb}} \lesssim 1$ hr. However, we note that an appreciable number of observed ELM WD bina-

ries with $M_{\text{He}} \lesssim 0.2 M_{\odot}$ have shorter P_{orb} than predicted by the stable mass transfer channel (Li et al. 2019), so it is possible the stable mass transfer channel may still produce high-entropy He WDs that are of interest to this work.

5. CONCLUSION

We have shown that mass transfer from a high-entropy He WD onto a massive CO WD can lead to a strong, first He flash. With higher donor entropy, the peak \dot{M} decreases, leading to a larger total accumulated He shell mass at ignition (see Section 2). For an initially $1.0 M_{\odot}$ accretor, the explored range of total accumulated He shell mass at ignition spans from 0.01 to $0.08 M_{\odot}$. By including CNO isotopes and a large nuclear network accounting for the reaction chain $^{12}\text{C}(p, \gamma)^{13}\text{N}(\alpha, p)^{16}\text{O}$ (Shen & Moore 2014), and by allowing superadiabaticity in the convection zone, we show that the resulting He flash can become dynamical (see Section 3).

Pending a successful double detonation, this scenario can explain some SNe Ia. For some thin-shell ($\lesssim 0.03 M_{\odot}$) models in our simulations, the resulting transient may be a spectroscopically normal SNe Ia, and thick-shell may produce peculiar SNe Ia (e.g., Polin et al. 2019; Townsley et al. 2019; Boos et al. 2021; Shen et al. 2021). Furthermore, our results provide a good match to the velocity of the hypervelocity WD D6-2 (Shen et al. 2018b; Bauer et al. 2021), and suggest that D6-2 must

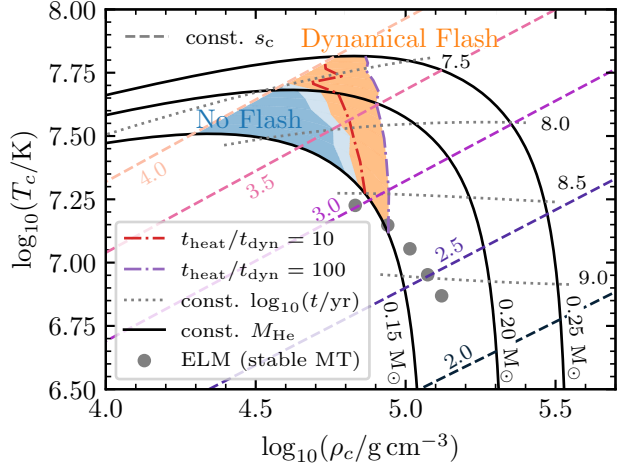


Figure 6. Central temperature and density trajectories of cooling He WDs of fixed masses from 0.15 to $0.25 M_{\odot}$ (black solid lines). Lines of constant entropy and cooling age are in dashed and dotted respectively. Blue region gives the parameter space where no He flash occurs, orange region where a He flash is possible with $\tau_{\text{heat}} \lesssim 100 \tau_{\text{dyn}}$, and light blue unknown due to our finite model grid. We also limit our models to $s_{c,\text{He}}^i / (N_{\Lambda} k_{\text{B}}) \leq 4.0$. Dot-dashed lines are estimates of where a He flash occurs with $\tau_{\text{heat}} = 10 \tau_{\text{dyn}}$ (red) and $100 \tau_{\text{dyn}}$ (purple). Circle markers are our ELM models following Sun & Arras (2018) which descend from the stable mass transfer channel.

have been high-entropy. We plan to study the impact of SN ejecta on high-entropy He WD donors like D6-2 in the near future, similarly to Bauer et al. (2019).

For non-dynamical He flashes that cause expansion of the accretor to Roche-lobe overflow, Shen (2015) has raised the possibility of a subsequent merger. Should this be the case, then the only surviving systems that continue to evolve to longer periods as AM CVn binaries (e.g. van Roestel et al. 2022), are those with initial entropies so large that no flash ever occurs.

In Section 4, we argue that these high-entropy He WDs that have a dynamical flash must result from a CE event. The unstable mass transfer begins near

the base of the RGB when the donor progenitor is still high-entropy, and ends with short orbital periods such that the newly formed He WD cannot cool before coming into contact again. Main sequence stars with masses $\approx 1.3 - 2.0 M_{\odot}$, an unseen companion with mass $\approx 1.0 M_{\odot}$, and orbital periods between 1 and 8 days are good candidates for producing the high-entropy He WDs of interest here. The short lifetimes (1.1 – 3.5 Gyr) of these main sequence stars may explain SNe Ia in a younger population.

We thank the referee for their constructive suggestions that have greatly improved our manuscript. We thank Evan Bauer, Adam Jermyn, Jared Goldberg, and Will Schultz for helpful conversations about running MESA and Evan Bauer in addition for sharing data of D6-2. We are grateful to Abigail Polin for helpful conversations about He detonation and thermonuclear supernovae, and Ken Shen in addition for helpful comments on an earlier draft. We thank Meng Sun for sharing her MESA inlists for modeling ELM WD formation. This work was supported, in part, by the National Science Foundation through grant PHY-1748958, and by the Gordon and Betty Moore Foundation through grant GBMF5076. Use was made of computational facilities purchased with funds from the National Science Foundation (CNS-1725797) and administered by the Center for Scientific Computing (CSC). The CSC is supported by the California NanoSystems Institute and the Materials Research Science and Engineering Center (MRSEC; NSF DMR 1720256) at UC Santa Barbara.

Software: MESA (v15140,v21.12.1,v22.05.1; Paxton et al. 2011, 2013, 2015, 2018, 2019; Jermyn et al. 2023), py_mesa_reader (Wolf & Schwab 2017), ipython/jupyter (Pérez & Granger 2007; Kluyver et al. 2016), matplotlib (Hunter 2007), NumPy (Harris et al. 2020), SciPy (Virtanen et al. 2020), Astropy (Astropy Collaboration et al. 2013, 2018), and Python from python.org .

REFERENCES

- Asplund, M., Grevesse, N., Sauval, A. J., & Scott, P. 2009, *ARA&A*, 47, 481, doi: [10.1146/annurev.astro.46.060407.145222](https://doi.org/10.1146/annurev.astro.46.060407.145222)
- Astropy Collaboration, Robitaille, T. P., Tollerud, E. J., et al. 2013, *A&A*, 558, A33, doi: [10.1051/0004-6361/201322068](https://doi.org/10.1051/0004-6361/201322068)
- Astropy Collaboration, Price-Whelan, A. M., Sipőcz, B. M., et al. 2018, *AJ*, 156, 123, doi: [10.3847/1538-3881/aabc4f](https://doi.org/10.3847/1538-3881/aabc4f)
- Bauer, E. B., Chandra, V., Shen, K. J., & Hermes, J. J. 2021, *ApJL*, 923, L34, doi: [10.3847/2041-8213/ac432d](https://doi.org/10.3847/2041-8213/ac432d)
- Bauer, E. B., & Kupfer, T. 2021, *ApJ*, 922, 245, doi: [10.3847/1538-4357/ac25f0](https://doi.org/10.3847/1538-4357/ac25f0)
- Bauer, E. B., Schwab, J., & Bildsten, L. 2017, *ApJ*, 845, 97, doi: [10.3847/1538-4357/aa7ffa](https://doi.org/10.3847/1538-4357/aa7ffa)
- Bauer, E. B., White, C. J., & Bildsten, L. 2019, *ApJ*, 887, 68, doi: [10.3847/1538-4357/ab4ea4](https://doi.org/10.3847/1538-4357/ab4ea4)

- Bildsten, L., Shen, K. J., Weinberg, N. N., & Nelemans, G. 2007, *ApJL*, 662, L95, doi: [10.1086/519489](https://doi.org/10.1086/519489)
- Blondin, S., Dessart, L., Hillier, D. J., & Khokhlov, A. M. 2017, *MNRAS*, 470, 157, doi: [10.1093/mnras/stw2492](https://doi.org/10.1093/mnras/stw2492)
- Blouin, S., Shaffer, N. R., Saumon, D., & Starrett, C. E. 2020, *ApJ*, 899, 46, doi: [10.3847/1538-4357/ab9e75](https://doi.org/10.3847/1538-4357/ab9e75)
- Boos, S. J., Townsley, D. M., Shen, K. J., Caldwell, S., & Miles, B. J. 2021, *ApJ*, 919, 126, doi: [10.3847/1538-4357/ac07a2](https://doi.org/10.3847/1538-4357/ac07a2)
- Brooks, J., Bildsten, L., Marchant, P., & Paxton, B. 2015, *ApJ*, 807, 74, doi: [10.1088/0004-637X/807/1/74](https://doi.org/10.1088/0004-637X/807/1/74)
- Brown, J. M., Garaud, P., & Stellmach, S. 2013, *ApJ*, 768, 34, doi: [10.1088/0004-637X/768/1/34](https://doi.org/10.1088/0004-637X/768/1/34)
- Brown, W. R., Kilic, M., Kenyon, S. J., & Gianninas, A. 2016, *ApJ*, 824, 46, doi: [10.3847/0004-637X/824/1/46](https://doi.org/10.3847/0004-637X/824/1/46)
- Burdge, K. B., El-Badry, K., Rappaport, S., et al. 2023, arXiv e-prints, arXiv:2303.13573, doi: [10.48550/arXiv.2303.13573](https://doi.org/10.48550/arXiv.2303.13573)
- Cassisi, S., Potekhin, A. Y., Salaris, M., & Pietrinferni, A. 2021, *A&A*, 654, A149, doi: [10.1051/0004-6361/202141425](https://doi.org/10.1051/0004-6361/202141425)
- Collins, C. E., Gronow, S., Sim, S. A., & Röpke, F. K. 2022, *MNRAS*, 517, 5289, doi: [10.1093/mnras/stac2665](https://doi.org/10.1093/mnras/stac2665)
- Cox, J. P., & Giuli, R. T. 1968, *Principles of stellar structure*
- De, K., Kasliwal, M. M., Polin, A., et al. 2019, *ApJL*, 873, L18, doi: [10.3847/2041-8213/ab0aec](https://doi.org/10.3847/2041-8213/ab0aec)
- Deloye, C. J., Taam, R. E., Winisdoerffer, C., & Chabrier, G. 2007, *MNRAS*, 381, 525, doi: [10.1111/j.1365-2966.2007.12262.x](https://doi.org/10.1111/j.1365-2966.2007.12262.x)
- Eggleton, P. P. 1983, *ApJ*, 268, 368, doi: [10.1086/160960](https://doi.org/10.1086/160960)
- Fink, M., Hillebrandt, W., & Röpke, F. K. 2007, *A&A*, 476, 1133, doi: [10.1051/0004-6361:20078438](https://doi.org/10.1051/0004-6361:20078438)
- Fink, M., Röpke, F. K., Hillebrandt, W., et al. 2010, *A&A*, 514, A53, doi: [10.1051/0004-6361/200913892](https://doi.org/10.1051/0004-6361/200913892)
- Fuller, J., & Lai, D. 2012, *ApJL*, 756, L17, doi: [10.1088/2041-8205/756/1/L17](https://doi.org/10.1088/2041-8205/756/1/L17)
- Fuller, J., Piro, A. L., & Jermyn, A. S. 2019, *MNRAS*, 485, 3661, doi: [10.1093/mnras/stz514](https://doi.org/10.1093/mnras/stz514)
- García-Senz, D., Bravo, E., & Woosley, S. E. 1999, *A&A*, 349, 177
- Glasner, S. A., Livne, E., Steinberg, E., Yalinewich, A., & Truran, J. W. 2018, *MNRAS*, 476, 2238, doi: [10.1093/mnras/sty421](https://doi.org/10.1093/mnras/sty421)
- Gronow, S., Collins, C., Ohlmann, S. T., et al. 2020, *A&A*, 635, A169, doi: [10.1051/0004-6361/201936494](https://doi.org/10.1051/0004-6361/201936494)
- Gronow, S., Collins, C. E., Sim, S. A., & Röpke, F. K. 2021, *A&A*, 649, A155, doi: [10.1051/0004-6361/202039954](https://doi.org/10.1051/0004-6361/202039954)
- Guillochon, J., Dan, M., Ramirez-Ruiz, E., & Rosswog, S. 2010, *ApJL*, 709, L64, doi: [10.1088/2041-8205/709/1/L64](https://doi.org/10.1088/2041-8205/709/1/L64)
- Harris, C. R., Millman, K. J., van der Walt, S. J., et al. 2020, *Nature*, 585, 357, doi: [10.1038/s41586-020-2649-2](https://doi.org/10.1038/s41586-020-2649-2)
- Hashimoto, M. A., Nomoto, K. I., Arai, K., & Kaminisi, K. 1986, *ApJ*, 307, 687, doi: [10.1086/164453](https://doi.org/10.1086/164453)
- Hoeflich, P., & Khokhlov, A. 1996, *ApJ*, 457, 500, doi: [10.1086/176748](https://doi.org/10.1086/176748)
- Hoyle, F., & Fowler, W. A. 1960, *ApJ*, 132, 565, doi: [10.1086/146963](https://doi.org/10.1086/146963)
- Hunter, J. D. 2007, *Computing In Science & Engineering*, 9, 90
- Iben, Icko, J., & Tutukov, A. V. 1991, *ApJ*, 370, 615, doi: [10.1086/169848](https://doi.org/10.1086/169848)
- Istrate, A. G., Marchant, P., Tauris, T. M., et al. 2016, *A&A*, 595, A35, doi: [10.1051/0004-6361/201628874](https://doi.org/10.1051/0004-6361/201628874)
- Jacobs, A. M., Zingale, M., Nonaka, A., Almgren, A. S., & Bell, J. B. 2016, *ApJ*, 827, 84, doi: [10.3847/0004-637X/827/1/84](https://doi.org/10.3847/0004-637X/827/1/84)
- Jermyn, A. S., Bauer, E. B., Schwab, J., et al. 2023, *ApJS*, 265, 15, doi: [10.3847/1538-4365/acae8d](https://doi.org/10.3847/1538-4365/acae8d)
- Kaplan, D. L., Bildsten, L., & Steinfadt, J. D. R. 2012, *ApJ*, 758, 64, doi: [10.1088/0004-637X/758/1/64](https://doi.org/10.1088/0004-637X/758/1/64)
- Kluyver, T., Ragan-Kelley, B., Pérez, F., et al. 2016, in *Positioning and Power in Academic Publishing: Players, Agents and Agendas: Proceedings of the 20th International Conference on Electronic Publishing*, IOS Press, 87
- Kolb, U., & Ritter, H. 1990, *A&A*, 236, 385
- Kromer, M., Sim, S. A., Fink, M., et al. 2010, *ApJ*, 719, 1067, doi: [10.1088/0004-637X/719/2/1067](https://doi.org/10.1088/0004-637X/719/2/1067)
- Landau, L. D., & Lifshitz, E. M. 1971, *The classical theory of fields*
- Langer, N., El Eid, M. F., & Fricke, K. J. 1985, *A&A*, 145, 179
- Leung, S.-C., & Nomoto, K. 2020, *ApJ*, 888, 80, doi: [10.3847/1538-4357/ab5c1f](https://doi.org/10.3847/1538-4357/ab5c1f)
- Li, Z., Chen, X., Chen, H.-L., & Han, Z. 2019, *ApJ*, 871, 148, doi: [10.3847/1538-4357/aaf9a1](https://doi.org/10.3847/1538-4357/aaf9a1)
- Livne, E. 1990, *ApJL*, 354, L53, doi: [10.1086/185721](https://doi.org/10.1086/185721)
- Livne, E., & Glasner, A. S. 1991, *ApJ*, 370, 272, doi: [10.1086/169813](https://doi.org/10.1086/169813)
- Marsh, T. R., Nelemans, G., & Steeghs, D. 2004, *MNRAS*, 350, 113, doi: [10.1111/j.1365-2966.2004.07564.x](https://doi.org/10.1111/j.1365-2966.2004.07564.x)
- Moll, R., & Woosley, S. E. 2013, *ApJ*, 774, 137, doi: [10.1088/0004-637X/774/2/137](https://doi.org/10.1088/0004-637X/774/2/137)
- Nelemans, G., Portegies Zwart, S. F., Verbunt, F., & Yungelson, L. R. 2001, *A&A*, 368, 939, doi: [10.1051/0004-6361:20010049](https://doi.org/10.1051/0004-6361:20010049)
- Neunteufel, P., Kruckow, M., Geier, S., & Hamers, A. S. 2021, *A&A*, 646, L8, doi: [10.1051/0004-6361/202040022](https://doi.org/10.1051/0004-6361/202040022)

- Neunteufel, P., Yoon, S. C., & Langer, N. 2017, *A&A*, 602, A55, doi: [10.1051/0004-6361/201630121](https://doi.org/10.1051/0004-6361/201630121)
- Nugent, P., Baron, E., Branch, D., Fisher, A., & Hauschildt, P. H. 1997, *ApJ*, 485, 812, doi: [10.1086/304459](https://doi.org/10.1086/304459)
- Pakmor, R., Kromer, M., Taubenberger, S., et al. 2012, *ApJL*, 747, L10, doi: [10.1088/2041-8205/747/1/L10](https://doi.org/10.1088/2041-8205/747/1/L10)
- Pakmor, R., Zenati, Y., Perets, H. B., & Toonen, S. 2021, *MNRAS*, 503, 4734, doi: [10.1093/mnras/stab686](https://doi.org/10.1093/mnras/stab686)
- Paxton, B., Bildsten, L., Dotter, A., et al. 2011, *ApJS*, 192, 3, doi: [10.1088/0067-0049/192/1/3](https://doi.org/10.1088/0067-0049/192/1/3)
- Paxton, B., Cantiello, M., Arras, P., et al. 2013, *ApJS*, 208, 4, doi: [10.1088/0067-0049/208/1/4](https://doi.org/10.1088/0067-0049/208/1/4)
- Paxton, B., Marchant, P., Schwab, J., et al. 2015, *ApJS*, 220, 15, doi: [10.1088/0067-0049/220/1/15](https://doi.org/10.1088/0067-0049/220/1/15)
- Paxton, B., Schwab, J., Bauer, E. B., et al. 2018, *ApJS*, 234, 34, doi: [10.3847/1538-4365/aaa5a8](https://doi.org/10.3847/1538-4365/aaa5a8)
- Paxton, B., Smolec, R., Schwab, J., et al. 2019, *ApJS*, 243, 10, doi: [10.3847/1538-4365/ab2241](https://doi.org/10.3847/1538-4365/ab2241)
- Pérez, F., & Granger, B. E. 2007, *Computing in Science & Engineering*, 9, 21
- Piersanti, L., Yungelson, L. R., Cristallo, S., & Tornambé, A. 2019, *MNRAS*, 484, 950, doi: [10.1093/mnras/stz033](https://doi.org/10.1093/mnras/stz033)
- Piersanti, L., Yungelson, L. R., & Tornambé, A. 2015, *MNRAS*, 452, 2897, doi: [10.1093/mnras/stv1452](https://doi.org/10.1093/mnras/stv1452)
- Piro, A. L. 2008, *ApJ*, 679, 616, doi: [10.1086/529363](https://doi.org/10.1086/529363)
- . 2015, *ApJ*, 801, 137, doi: [10.1088/0004-637X/801/2/137](https://doi.org/10.1088/0004-637X/801/2/137)
- Polin, A., Nugent, P., & Kasen, D. 2019, *ApJ*, 873, 84, doi: [10.3847/1538-4357/aafb6a](https://doi.org/10.3847/1538-4357/aafb6a)
- Ramsay, G., Green, M. J., Marsh, T. R., et al. 2018, *A&A*, 620, A141, doi: [10.1051/0004-6361/201834261](https://doi.org/10.1051/0004-6361/201834261)
- Scherbak, P., & Fuller, J. 2023, *MNRAS*, 518, 3966, doi: [10.1093/mnras/stac3313](https://doi.org/10.1093/mnras/stac3313)
- Schwab, J., Bildsten, L., & Quataert, E. 2017, *MNRAS*, 472, 3390, doi: [10.1093/mnras/stx2169](https://doi.org/10.1093/mnras/stx2169)
- Shen, K. J. 2015, *ApJL*, 805, L6, doi: [10.1088/2041-8205/805/1/L6](https://doi.org/10.1088/2041-8205/805/1/L6)
- Shen, K. J., & Bildsten, L. 2009, *ApJ*, 699, 1365, doi: [10.1088/0004-637X/699/2/1365](https://doi.org/10.1088/0004-637X/699/2/1365)
- . 2014, *ApJ*, 785, 61, doi: [10.1088/0004-637X/785/1/61](https://doi.org/10.1088/0004-637X/785/1/61)
- Shen, K. J., Boos, S. J., Townsley, D. M., & Kasen, D. 2021, *ApJ*, 922, 68, doi: [10.3847/1538-4357/ac2304](https://doi.org/10.3847/1538-4357/ac2304)
- Shen, K. J., Kasen, D., Miles, B. J., & Townsley, D. M. 2018a, *ApJ*, 854, 52, doi: [10.3847/1538-4357/aaa8de](https://doi.org/10.3847/1538-4357/aaa8de)
- Shen, K. J., Kasen, D., Weinberg, N. N., Bildsten, L., & Scannapieco, E. 2010, *ApJ*, 715, 767, doi: [10.1088/0004-637X/715/2/767](https://doi.org/10.1088/0004-637X/715/2/767)
- Shen, K. J., & Moore, K. 2014, *ApJ*, 797, 46, doi: [10.1088/0004-637X/797/1/46](https://doi.org/10.1088/0004-637X/797/1/46)
- Shen, K. J., Boubert, D., Gänsicke, B. T., et al. 2018b, *ApJ*, 865, 15, doi: [10.3847/1538-4357/aad55b](https://doi.org/10.3847/1538-4357/aad55b)
- Sim, S. A., Fink, M., Kromer, M., et al. 2012, *MNRAS*, 420, 3003, doi: [10.1111/j.1365-2966.2011.20162.x](https://doi.org/10.1111/j.1365-2966.2011.20162.x)
- Sim, S. A., Röpke, F. K., Hillebrandt, W., et al. 2010, *ApJL*, 714, L52, doi: [10.1088/2041-8205/714/1/L52](https://doi.org/10.1088/2041-8205/714/1/L52)
- Spruit, H. C. 2002, *A&A*, 381, 923, doi: [10.1051/0004-6361:20011465](https://doi.org/10.1051/0004-6361:20011465)
- Sun, M., & Arras, P. 2018, *ApJ*, 858, 14, doi: [10.3847/1538-4357/aab9a4](https://doi.org/10.3847/1538-4357/aab9a4)
- Temmink, K. D., Pols, O. R., Justham, S., Istrate, A. G., & Toonen, S. 2023, *A&A*, 669, A45, doi: [10.1051/0004-6361/20224413710.48550/arXiv.2209.12707](https://doi.org/10.1051/0004-6361/20224413710.48550/arXiv.2209.12707)
- Townsley, D. M., Miles, B. J., Shen, K. J., & Kasen, D. 2019, *ApJL*, 878, L38, doi: [10.3847/2041-8213/ab27cd](https://doi.org/10.3847/2041-8213/ab27cd)
- van Roestel, J., Kupfer, T., Green, M. J., et al. 2022, *MNRAS*, 512, 5440, doi: [10.1093/mnras/stab2421](https://doi.org/10.1093/mnras/stab2421)
- Virtanen, P., Gommers, R., Oliphant, T. E., et al. 2020, *Nature Methods*, 17, 261, doi: [10.1038/s41592-019-0686-2](https://doi.org/10.1038/s41592-019-0686-2)
- Wolf, B., & Schwab, J. 2017, *wmwoff/py_mesa_reader: Interact with MESA Output, 0.3.0*, Zenodo, doi: [10.5281/zenodo.826958](https://doi.org/10.5281/zenodo.826958)
- Wong, T. L. S., & Bildsten, L. 2021, *ApJ*, 923, 125, doi: [10.3847/1538-4357/ac2b2a](https://doi.org/10.3847/1538-4357/ac2b2a)
- Woosley, S. E., & Kasen, D. 2011, *ApJ*, 734, 38, doi: [10.1088/0004-637X/734/1/38](https://doi.org/10.1088/0004-637X/734/1/38)
- Woosley, S. E., & Weaver, T. A. 1994, *ApJ*, 423, 371, doi: [10.1086/173813](https://doi.org/10.1086/173813)
- Yoon, S. C., Langer, N., & Scheithauer, S. 2004, *A&A*, 425, 217, doi: [10.1051/0004-6361:20040327](https://doi.org/10.1051/0004-6361:20040327)
- Zingale, M., Nonaka, A., Almgren, A. S., et al. 2013, *ApJ*, 764, 97, doi: [10.1088/0004-637X/764/1/97](https://doi.org/10.1088/0004-637X/764/1/97)
- Zorotovic, M., Schreiber, M. R., Gänsicke, B. T., & Nebot Gómez-Morán, A. 2010, *A&A*, 520, A86, doi: [10.1051/0004-6361/20091365810.48550/arXiv.1006.1621](https://doi.org/10.1051/0004-6361/20091365810.48550/arXiv.1006.1621)